Electrochemistry Communications 151 (2023) 107496

Contents lists available at ScienceDirect

Electrochemistry Communications

journal homepage: www.elsevier.com/locate/elecom

A direct method to quantify lithium plating on graphite negative electrode of commercial Li-ion cells

Emanuele Gucciardi [a,*], Francesco Torre [a,*], Maria A. Cabañero [a], Laura Oca [b], Emilie Bekaert [a]

[a] Centre for Cooperative Research on Alternative Energies (CIC energiGUNE), Basque Research and Technology Alliance (BRTA), Alava Technology Park, Albert Einstein 48, 01510 Vitoria-Gasteiz, Spain
[b] Mondragon Unibertsitatea, Electronic and Computer Science Department, Loramendi 4, 20500 Mondragon, Basque Country, Spain

ARTICLE INFO

Keywords:
Li-ion battery
Lithium plating
Lithium quantification
Battery aging
Safety

ABSTRACT

The deposition of metallic lithium is a degradation mechanism, also known as lithium plating, that might occur at the negative electrode surface of Li-ion battery cell, especially during fast charging, low temperature charging and high state of charge. The loss of cyclable lithium may lead to irreversible capacity fade and might also bring significant safety hazards. In this context, the experimental quantification of plated lithium on the negative electrode surface could be used to accurately validate electrochemical and physical models that might be used to predict plated lithium without cell opening. Also, the determination of plated Li may help in the evaluation of the safety and aging of commercial cells from different manufacturers for a specific application. This work shows a fast and cost-effective method that can be used to quantify plated lithium on commercial Li-ion battery graphite electrodes.

1. Introduction

Lithium-ion batteries (LIBs), represent today the most used electrochemical power source and essential element in many consumer electronics, stationary and mobility applications [1]. Its wide use is justified by the high energy and volumetric densities, low self-discharge, long cycling life reduced cost when compared to, cyclability and higher voltage than other battery technologies [2,3]. However, LIBs lifetime is reduced by non-desirable side reactions that lead to an increase of the internal resistance. This has an impact on the available power and causes capacity fade, leading to a premature battery end-of-life (EoL) [4].

The main aging mechanisms that occur at the negative electrode are mainly caused by the solid electrolyte interface (SEI) growth, metallic lithium deposition, also called lithium plating, and electrolyte decomposition [5,6]. All these mechanisms trap lithium in a different manner, but all lead to a loss of lithium inventory (LLI), decreasing the durability of the cell [7].

Among these mechanisms, Li plating is considered one of the main degradation mechanisms occurring under certain circumstances, i.e., battery fast-charging [8,9], low temperatures charge [10,11], poor negative to positive electrode mass ratio or long-term cycling [7,12–15].

All these conditions to which the negative electrode may be subjected will produce a local anode polarization that brings its potential below 0 V vs Li/Li^+ causing the lithium reduction in the form of Li^0 on the negative electrode. In addition, one of the major concerns about lithium plating is that it might lead to the formation of dendrites causing internal short circuits, ending up with important safety hazards such as fire and/or explosion [16].

Moreover, deposited metallic Li can be electrochemically inactive and after its reaction with the electrolyte, can bring to the formation of new SEI then causing further capacity loss [9,12,17].

The accurate determination of plated lithium is crucial for improving the performance of LIBs and developing aging models that can predict the EoL of a battery without opening it. Quantifying plated lithium can also help evaluate commercial cells for specific applications under conditions where plating is expected.

Currently, available methods that determine plated lithium could be classified as non-invasive and invasive methods. Non-invasive methods are usually included in those electrochemical approaches that are able to detect lithium deposition. These methods are mainly based on differential voltage analysis on full cells [9,18], electrochemical impedance spectroscopy (EIS) measurements [19] and *in-operando* acoustic detection [20].

* Corresponding authors.
E-mail addresses: egucciardi@cicenergigune.com (E. Gucciardi), ftorre@cicenergigune.com (F. Torre).

https://doi.org/10.1016/j.elecom.2023.107496
Received 22 March 2023; Received in revised form 25 April 2023; Accepted 27 April 2023
Available online 5 May 2023

Within the invasive methods can be included some *in-operando* electrochemical characterization. In fact, by including a reference electrode in the studied cell [21] it is possible to measure the positive and negative electrode potential. In this manner, it is possible to accurately know when the negative electrode potential goes below 0 V and, depending on the time spent in that region, a correlation to the plated lithium that is generated could be determined [22,23]. However, a reference electrode is not yet implemented in current commercial cells and research to include a reference electrode into battery cells is still ongoing due to its stability, position, processing and cost [24,25].

Also, other invasive post-mortem methods able to detect plated lithium based on Raman [26] and on solid-state nuclear magnetic resonance (NMR) were developed [11,27].

Nonetheless, both non-invasive and invasive methods are powerful tools that are able to detect plated lithium but are less efficient to quantify it, since the measurement is restricted to a small area of the electrode. Moreover, the quantitative determination of plated Li results is somehow tricky due to complexities in the discrimination between metallic Li plated irreversibly at the negative electrode surface, Li irreversibly lost during the SEI formation and some remaining intercalated Li into graphite or reversible plated Li [16]. Therefore, new methods for quantitative determination of lithium deposition are needed.

In literature there are few examples of post-mortem Li-plating quantification. For example, Ghanbari et Al. introduced a method for detecting and characterizing plated lithium on graphite anodes of LIBs by means of glow discharge optical emission spectroscopy (GD-OES) depth profiling [28]. Instead, Fang et Al. propose to detect dead Li on a Li//Cu cell for solid-state battery using titration gas chromatography (TGC) to quantify the contribution of plated Li to the total amount of trapped lithium [29].

Other methods involve massive Li deposition on commercial cells [16,23,30] and dilatation methods. The last one can be applied only to pouch cell format [31,32].

Here we present a new cost-effective, fast, and direct method able to accurately quantify metallic lithium deposited on LIB graphite electrodes by measuring the H_2 produced in the reaction of H_2O with the plated metallic lithium.

2. Materials and methods

2.1. Sample preparation

For the research presented in this paper, 2 commercial cylindrical cells with a nominal capacity of 2.85 Ah with reference number INR-18650-M29 of the manufacturer LG CHEM were used.

In order to trigger the plating formation on the negative electrode, one cell was cycled at −20 °C in a VÖTSCH climatic chamber with a standard protocol which includes a discharge current of 1C and a charge current of 1.6 C for 42 cycles. The cell is cycled with CCCV charge and CC discharge protocol between 4.2 V and 2.5 V and with a BT-LAB® battery tester (BIO-LOGIC). The other cell is left uncycled and used as a reference.

Once the two cells are discharged at 2.5 V, are both dismantled inside a glove box (Jacomex) with oxygen (<0.1 ppm) and water (<0.1 ppm) controlled environment. From each cell, two portions of the double side coated anode of 5x5 cm^2 dimension from each cell are harvested, weighted, and stored in a vial. The negative electrode harvested from the fresh battery should not contain plated lithium but only the initial SEI layer formation. For simplicity, the two samples are named fresh and aged, respectively.

Samples were collected from the same zones of the negative electrode for both batteries without washing to prevent material loss or surface chemistry alteration. The weight of each electrode was recorded before introducing them into the reactor to determine the amount of electrochemically inactive Li relative to the electrode material.

2.2. Experimental setup for Li plating detection

Fig. 1 shows the scheme of the lab-made system used to quantify metallic lithium. This small equipment consists of a quartz reactor with a Teflon plug that is connected to a three-way Swagelok-type, gas-tight setup. The system includes a porous rubber septum to allow the introduction of water by means of a syringe, as well as a ball valve to fill/vent the reactor. The top part is connected to a Clark-type hydrogen microsensor (Unisense, Denmark) which is sensitive to the H_2 partial pressure and has a detection limit of $\approx 10^{-2}$ vol%. This device includes a Pt sensing anode that is polarized against an internal reference electrode thanks to a high-sensitivity picometer (UniAmp). An H_2-permeable membrane allows the diffusion of H_2 to the sensor's anode, where its oxidation produces a signal that is recorded through a dedicated software.

2.3. Experimental methodology

The H_2 microsensor is calibrated to quantify the amount of deposited metallic Li on fresh and aged negative electrode samples. The sensor has a linear response and can be calibrated using a two-point calibration, but a four-point calibration was performed to ensure better accuracy and to account for any experimental error related to the setup or methodology used as shown in the supporting info (SI). To build the calibration curve, increasing amounts of metallic Li (China Energy Lithium Co., Ltd) were initially measured, and the resulting H_2 sensor outputs were used to establish the curve. This calibration curve was then used to quantify the unknown amount of deposited metallic Li on the fresh and aged negative electrode samples. The sample loading process shown in Fig. 1, takes place in four stages: i) bringing the lab-made system inside a glove box; ii) inserting the material to be tested into the reactor in an argon

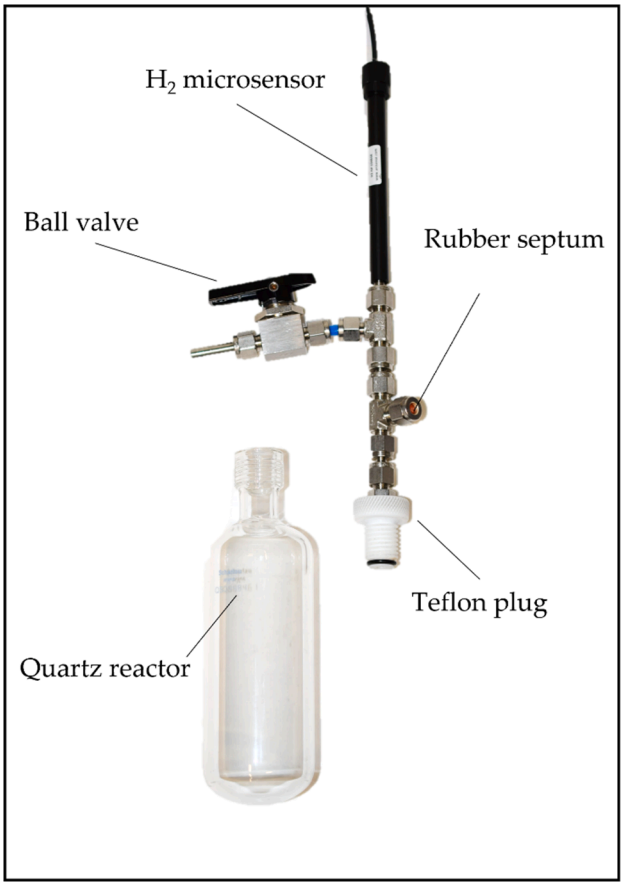

Fig. 1. Scheme of the lab-made system used for metallic Li quantification.

atmosphere; iii) connecting the H_2 microsensor back to its original position while vigorously flowing argon through the reactor, iv) introducing a water excess through a syringe. To avoid a temperature increase and reduce the formation of water vapor during the reaction, the bottom of the reactor was kept inside an ice bath (see supporting info.). When the reaction was completed, the ball valve was opened to bleed off the reactor and suddenly closed. This step eliminated the overpressure generated by the H_2 release and took the total pressure of the system back to 1 atm. This is necessary to not overestimate the H_2 concentration (see supporting info.). Data acquisition was set at 1 point every second, and the average of the last 20 experimental points was used as the final value for sensor calibration and quantification of plated Li.

3. Results and discussions

Negative electrode portions from fresh and aged cells are shown in Fig. 2a and 2b, respectively. The fresh negative electrode has an opaque, graphite-colored surface where no metallic Li is expected. The aged negative electrode appears silvery and homogeneous, indicating Li plating.

Between the species that can be present on the graphite electrode surface, only Li and LiH can produce H_2 as a product of the reaction with H_2O. In fact, as was described by Feng et al. [29], only the presence of LiH compound could affect the quantification of metallic Li. But this compound is mainly found on Li metal batteries where the H_2, produced by the reduction of H_2O traces or protic electrolyte oxidation species from the cathode, reacts with big amounts of metallic Li to give LiH [33–35].

Thus, the metallic Li quantification was indirectly determined by backtracking the H_2 released in the form of gas by the reaction of Li with an excess of H_2O (1).

$$2Li + 2H_2O \rightarrow 2LiOH + H_2 \uparrow \quad (1)$$

To elucidate the operating principle of the adopted methodology, a description of the chemical-physical process taking place inside the reactor is given.

During reaction (1), the released H_2 mixes with the Ar already present in the reactor to give an Ar/H_2 gaseous solution. As the initial moles of Ar (mol_{Ar}) are the same for every experiment ($11.86 \cdot 10^{-2}$ according to the ideal gas law), the resulting H_2 molar fraction (χH_2) is proportional to the moles of metallic Li (mol_{Li}).

Table 1
Data used for the calibration with metallic Li reported in Fig. 3b. The H_2 concentrations expected for the different Li amounts are also reported.

Li (mg)	H_2 microsensor signal (mV)	χH_2 (mol.%) *
4.5	99.0 ± 0.4	2.66
10.6	168.4 ± 0.4	6.05
19.0	234.3 ± 0.3	10.34
41.4	467.2 ± 0.5	20.88

* Calculated according to the ideal gas law. T = 20 °C, P = 1 atm and V = 0.293 L.

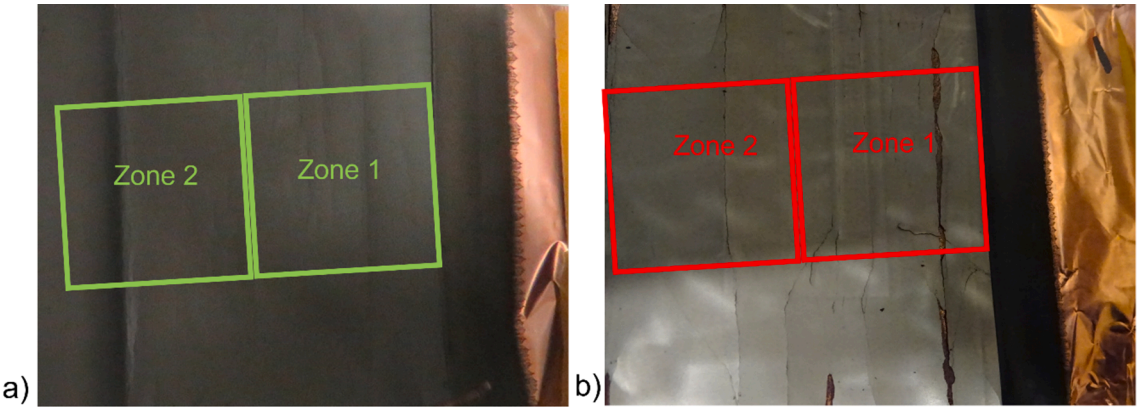

Fig. 2. Electrode zones collected from (a) fresh cell negative electrode and (b) aged cell negative electrode used for the plated Li quantification test.

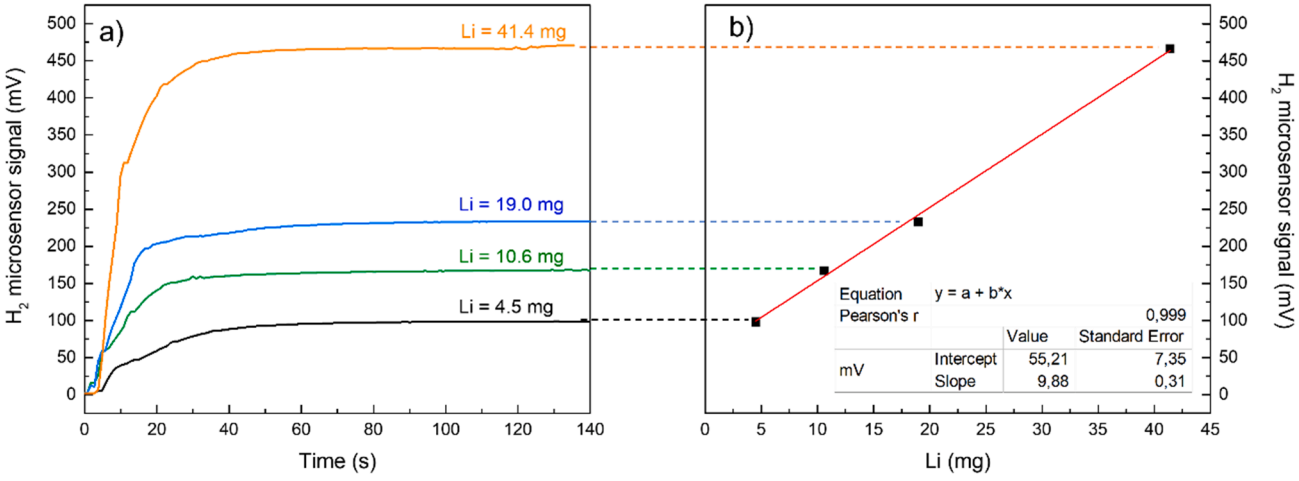

Fig. 3. (a) H_2 microsensor profiles acquired *in situ* for different known amounts of pure Li. (b) Calibration curve (mV vs mg of Li) built by using the average plateau values taken from the H_2 microsensor profiles.

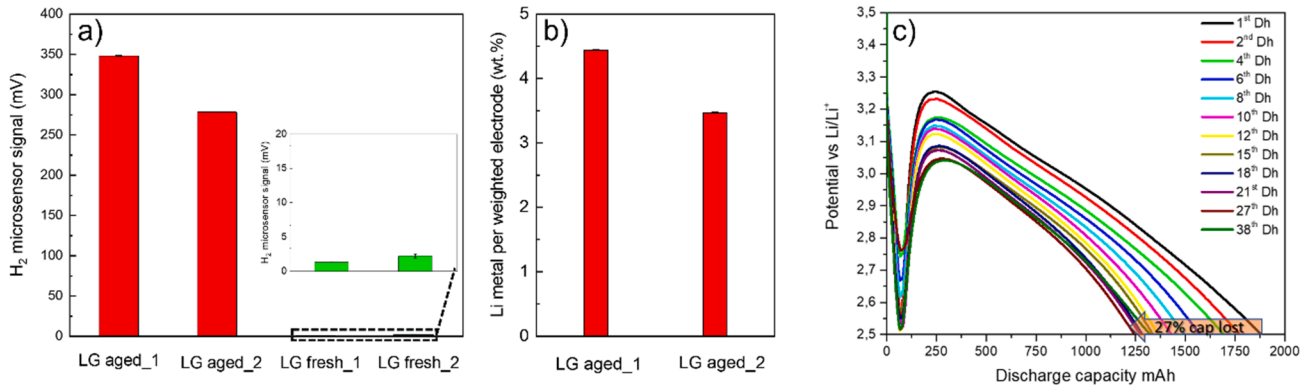

Fig. 4. (a) H_2 microsensor values acquired from the two zones collected from aged and fresh negative electrodes; (b) Given percentage of metallic Li per electrode material for the two portions of aged negative electrodes; (c) Galvanostatic discharge capacity lost from the full cell during −20 °C cycling at 1C current.

Table 2
Data obtained for the aged and fresh negative electrode portions.

Sample	H_2 microsensor signal (mV)**	Li (mg)	Li/electrode material (wt.%)	Dead Li mAh /cm^2	% capacity loss
LG-20_1	348.0 ± 0.7	29.8 ± 0.07	4.44 ± 0.01	1.15	29
LG-20_2	278.0 ± 0.5	22.8 ± 0.05	3.47 ± 0.01	0.88	22
LG25_1	1.3 ± 0.2	≪LoQ*	-	-	-
LG25_2	2.2 ± 0.3	≪LoQ*	-	-	-

* LoQ = Limit of Quantification. **The baseline value has been subtracted.

$$\chi H_2 = \frac{0.5 mol_{Li}}{0.5 mol_{Li} + mol_{Ar}} \quad (2)$$

where the coefficient 0.5 considers the stoichiometry of the reaction (1). Knowing the χH_2, in equation (2) can be used to backtrack the unknown amount of Li.

It is worth remembering that the H_2 microsensor used in this work is sensible to the H_2 partial pressure (pH_2), which is related to χH_2 as follows:

$$pH_2 = \chi H_2 \cdot P \quad (3)$$

where P is the total pressure. However, as the pressure inside the reactor was kept constant at 1 atm (see Section 2.3), the H_2 partial pressure coincides with the H_2 molar fraction. In such a way, the H_2 microsensor can be used to directly measure χH_2, and the amount of plated Li can be calculated from equation (2).

The sensor and the system are calibrated with four known amounts of pure metallic Li, namely 4.5, 10.6, 19.0 and 41.4 mg.

Fig. 3a shows the H_2 microsensor data acquired *in situ* for the different pure Li samples. In all cases, the sensor signal rapidly increases and approaches a plateau in approximately 1 min. For each experiment, <3 min were sufficient to achieve a stable signal (< ± 1 mV). The average H_2 microsensor signals (mV) obtained for the different amounts of pure Li are reported in Table 1, together with the uncertainty related to the sensor fluctuations.

The 0.999 Pearson correlation coefficient (r), which value is shown in the table in Fig. 3b, confirms the linear response of the H_2 microsensor in the explored concentration range (Table 1). The microsensor signal is directly proportional to the χH_2, which is also directly proportional to the amount of Li. Thus, the calibration curve can be directly used to calculate an unknown amount of metallic Li.

To test the device's response, two experiments per cell were conducted on a 5 × 5 cm^2 portion of fresh and aged negative electrode (Fig. 2a and Fig. 2b). Reproducibility was verified by repeating the test on another sample from zone 2 of both electrodes. The samples were sealed in the reactor one by one following the procedure described previously. Fig. 4a shows the aged sample reacted vigorously with water injection, producing a rapid and stable H_2 microsensor signal around 350 mV and 280 mV for zones 1 and 2, respectively. The inlet of Fig. 4a also shows the fresh sample which produced a slight signal increase close to the sensor limit of detection (2.45 mV) and below the limit of quantification (7.44 mV), which is negligible and could be attributed to some little baseline fluctuation during the measurement. LoD and LoQ calculations are shown in the SI.

Finally, the quantification of metallic Li was done by means of the previously built calibration curve and the results are graphically reported in Fig. 4b. The quantification of deposited Li is referred to the total weight of the electrode material and the values are resumed in Table 2. The two portions of aged negative electrode present 4.44 wt% and 3.47 wt% of metallic Li. These values are in the same range of some reported values present in literature as reported in Table S3 in the SI.

Starting from the concept that the capacity loss for the battery aged at extremely low temperature is mainly due to Li-plating, as previously reported by other researchers [36], we aim to confirm that the measured amount of Li is consistent with the observed capacity loss during battery cycling. Therefore, we measured the total area of the electrode, which was 664 cm^2. Thus, the capacity related to the area of the harvested electrode is estimated to be 3.95 mAh/cm^2. Using the Faraday law, we determined that the Li quantity measured in 25 cm^2 of the double-coated electrode used for our experiment corresponds to 1.15 and 0.88 mAh/cm^2 for each harvested zone respectively. These values indicate that 22 % and 29 % of the initial capacity of the electrode has been lost as dead Li, which agrees with the total capacity loss of the cell, which is determined to be 27.7 % as shown in Fig. 4c. However, these observed differences between the 2 zones of the negative electrode might be attributed to a non-homogenous behavior of Li plating in cylindrical cells that has been widely reported in the literature [37,38].

4. Conclusions

In this work, a method for metallic lithium quantification on commercial LIBs negative electrodes is presented using a small lab-made device. This device is based on a commercial sensor and can be

calibrated by using known amounts of pure metallic Li. The validated methodology is used to quantify deposited metallic Li on a commercial battery where plated Li was induced, and a fresh battery was tested as a reference. The knowledge of this parameter can be used in models to predict the EoL of a battery and can provide important information regarding Li-ion cell safety. This method allows fast and accurate quantification and can be applied to a broad range of other battery systems, supporting the manufacture of safer batteries with better cycling life performances. Future studies will aim to safely apply this methodology to the entire electrode area.

CRediT authorship contribution statement

Emanuele Gucciardi: Visualization, Conceptualization, Methodology, Investigation, Supervision, Writing – original draft. **Francesco Torre:** Conceptualization, Data curation, Methodology, Investigation, Writing – original draft. **Maria A. Cabañero:** Investigation, Writing – review & editing. **Laura Oca:** Investigation, Writing – review & editing. **Emilie Bekaert:** Supervision, Writing – review & editing.

Declaration of Competing Interest

The authors declare that they have no known competing financial interests or personal relationships that could have appeared to influence the work reported in this paper.

Data availability

Data will be made available on request.

Acknowledgement

The authors want to acknowledge the entity that funded this work that was financially supported by the Basque Government through the Elkartek program CICe2021 (KK-2021/00064). The authors also want to acknowledge the dedication of Ander Celaya and Bruno Correa for their technical support.

Appendix A. Supplementary material

Supplementary data to this article can be found online at https://doi.org/10.1016/j.elecom.2023.107496.

References

[1] M. Li, J. Lu, Z. Chen, K. Amine, Adv. Mater. 30 (2018) 1–24, https://doi.org/10.1002/adma.201800561.
[2] C. Julien, A. Mauger, A. Vijh, K. Zaghib, 2015; ISBN 9783319191089.
[3] N. Nitta, F. Wu, J.T. Lee, G. Yushin, Mater. Today 18 (2015) 252–264, https://doi.org/10.1016/j.mattod.2014.10.040.
[4] T. Waldmann, A. Iturrondobeitia, M. Kasper, N. Ghanbari, F. Aguesse, E. Bekaert, L. Daniel, S. Genies, I.J. Gordon, M.W. Löble, J. Electrochem. Soc. 163 (2016) A2149–A2164, https://doi.org/10.1149/2.1211609jes.
[5] R. Xiong, Y. Pan, W. Shen, H. Li, F. Sun, Renew. Sustain. Energy Rev. 131 (2020), 110048, https://doi.org/10.1016/j.rser.2020.110048.
[6] T.C. Bach, S.F. Schuster, E. Fleder, J. Müller, M.J. Brand, H. Lorrmann, A. Jossen, G.J. Sextl, Energy Storage 5 (2016) 212–223, https://doi.org/10.1016/j.est.2016.01.003.
[7] D. Anseán, M. Dubarry, A. Devie, B.Y. Liaw, V.M. García, J.C. Viera, M. González, J. Power Sources 356 (2017) 36–46, https://doi.org/10.1016/j.jpowsour.2017.04.072.
[8] Z.M. Konz, Z.M. Konz, E.J. McShane, E.J. McShane, B.D. McCloskey, B. D. McCloskey, ACS Energy Lett. 5 (2020) 1750–1757, https://doi.org/10.1021/acsenergylett.0c00831.
[9] I.D. Campbell, M. Marzook, M. Marinescu, G.J. Offer, J. Electrochem. Soc. 166 (2019) A725–A739, https://doi.org/10.1149/2.0821904jes.
[10] M. Petzl, M. Kasper, M.A. Danzer, J. Power Sources 275 (2015) 799–807, https://doi.org/10.1016/j.jpowsour.2014.11.065.
[11] H. Ge, T. Aoki, N. Ikeda, S. Suga, T. Isobe, Z. Li, Y. Tabuchi, J. Zhang, J. Electrochem. Soc. 164 (2017) A1050–A1060, https://doi.org/10.1149/2.0461706jes.
[12] X.-G. Yang, Y. Leng, G. Zhang, S. Ge, C.-Y. Wang, J. Power Sources 360 (2017) 28–40, https://doi.org/10.1016/j.jpowsour.2017.05.110.
[13] F. Ringbeck, C. Rahe, G. Fuchs, D.U. Sauer, J. Electrochem. Soc. 167 (2020), 090536, https://doi.org/10.1149/1945-7111/ab8f5a.
[14] Q. Li, T. Yi, X. Wang, H. Pan, B. Quan, T. Liang, X. Guo, X. Yu, H. Wang, X. Huang, et al., Nano Energy 63 (2019), 103895, https://doi.org/10.1016/j.nanoen.2019.103895.
[15] J.S. Edge, S. O'Kane, R. Prosser, N.D. Kirkaldy, A.N. Patel, A. Hales, A. Ghosh, W. Ai, J. Chen, J. Yang, et al., Lithium Ion Battery Degradation: What You Need to Know, Phys. Chem. Chem. Phys. 23 (2021) 8200–8221, https://doi.org/10.1039/d1cp00359c.
[16] T. Waldmann, B.I. Hogg, M. Wohlfahrt-Mehrens, Li Plating as Unwanted Side Reaction in Commercial Li-Ion Cells – A Review, J. Power Sources 384 (2018) 107–124, https://doi.org/10.1016/j.jpowsour.2018.02.063.
[17] X. Zhao, Y. Yin, Y. Hu, S.Y. Choe, J. Power Sources 418 (2019) 61–73, https://doi.org/10.1016/j.jpowsour.2019.02.001.
[18] X.G. Yang, S. Ge, T. Liu, Y. Leng, C.Y. Wang, J. Power Sources 395 (2018) 251–261, https://doi.org/10.1016/j.jpowsour.2018.05.073.
[19] N. Meddings, M. Heinrich, F. Overney, J.S. Lee, V. Ruiz, E. Napolitano, S. Seitz, G. Hinds, R. Raccichini, M. Gaberšček, J. Power Sources (2020) 480, https://doi.org/10.1016/j.jpowsour.2020.228742.
[20] C. Bommier, W. Chang, Y. Lu, J. Yeung, G. Davies, R. Mohr, M. Williams, D. Steingart, Cell Reports Phys. Sci. 1 (2020), 100035, https://doi.org/10.1016/j.xcrp.2020.100035.
[21] J. Liu, Z. Chu, H. Li, D. Ren, Y. Zheng, L. Lu, X. Han, M. Ouyang, Int. J. Energy Res. 45 (2021) 7918–7932, https://doi.org/10.1002/er.6375.
[22] S.P. Rangarajan, Y. Barsukov, P.P.J. Mukherjee, Mater. Chem. A 7 (2019) 20683–20695, https://doi.org/10.1039/c9ta07314k.
[23] T. Waldmann, M. Kasper, M. Wohlfahrt-Mehrens, Electrochim. Acta 178 (2015) 525–532, https://doi.org/10.1016/j.electacta.2015.08.056.
[24] Y. Li, X. Han, X. Feng, Z. Chu, X. Gao, R. Li, J. Du, L. Lu, M. Ouyang, J. Power Sources 481 (2021), 228933, https://doi.org/10.1016/j.jpowsour.2020.228933.
[25] V. Pande, A. Abbasalinejad, J. Hammond, J. Christensen, S.U. Kim, J. Electrochem. Soc. 168 (2021), 090534, https://doi.org/10.1149/1945-7111/ac2469.
[26] M.A. Cabañero, M. Hagen, E. Quiroga-González, Electrochim. Acta 374 (2021), 137487, https://doi.org/10.1016/J.ELECTACTA.2020.137487.
[27] Y.C. Hsieh, M. Leißing, S. Nowak, B.J. Hwang, M. Winter, G. Brunklaus, Cell Reports Phys. Sci. 1 (2020), 100139, https://doi.org/10.1016/j.xcrp.2020.100139.
[28] N. Ghanbari, T. Waldmann, M. Kasper, P. Axmann, M. Wohlfahrt-Mehrens, ECS Electrochem. Lett. 4 (2015) A100–A102, https://doi.org/10.1149/2.0041509eel.
[29] C. Fang, J. Li, M. Zhang, Y. Zhang, F. Yang, J.Z. Lee, M.H. Lee, J. Alvarado, M. A. Schroeder, Y. Yang, et al., Quantifying Inactive Lithium in Lithium Metal Batteries, Nature 572 (2019) 511–515, https://doi.org/10.1038/s41586-019-1481-z.
[30] M. Fleischhammer, T. Waldmann, G. Bisle, B.I. Hogg, M. Wohlfahrt-Mehrens, J. Power Sources 274 (2015) 432–439, https://doi.org/10.1016/j.jpowsour.2014.08.135.
[31] B. Bitzer, A. Gruhle, J. Power Sources 262 (2014) 297–302, https://doi.org/10.1016/j.jpowsour.2014.03.142.
[32] M. Bauer, M. Wachtler, H. Stöwe, J.V. Persson, M.A. Danzer, J. Power Sources 317 (2016) 93–102, https://doi.org/10.1016/j.jpowsour.2016.03.078.
[33] M. Metzger, B. Strehle, S. Solchenbach, H.A. Gasteiger, J. Electrochem. Soc. 163 (2016) A798–A809, https://doi.org/10.1149/2.1151605jes.
[34] G. Xu, J. Li, C. Wang, X. Du, D. Lu, B. Xie, X. Wang, C. Lu, H. Liu, S. Dong, et al., Angew. Chemie 133 (2021) 7849–7855, https://doi.org/10.1002/ange.202013812.
[35] L. Huang, G. Xu, X. Du, J. Li, B. Xie, H. Liu, P. Han, S. Dong, G. Cui, L. Chen, Adv. Sci. 8 (2021) 1–11, https://doi.org/10.1002/advs.202100676.
[36] T. Waldmann, M. Wilka, M. Kasper, M. Fleischhammer, M. Wohlfahrt-Mehrens, J. Power Sources 262 (2014) 129–135, https://doi.org/10.1016/j.jpowsour.2014.03.112.
[37] T. Sun, T. Shen, Y. Zheng, D. Ren, W. Zhu, J. Li, Y. Wang, K. Kuang, X. Rui, S. Wang, L. Wang, X. Han, L. Lu, Electrochim. Acta 425 (2022), 140701, https://doi.org/10.1016/j.electacta.2022.140701.
[38] M. Storch, J.P. Fath, J. Sieg, D. Vrankovic, C. Krupp, B. Spier, R.J. Riedel, Energy Storage 41 (2021), 102887, https://doi.org/10.1016/j.est.2021.102887.